






RESEARCH REPORT

ArcheD, a residual neural network for prediction of cerebrospinal fluid amyloid-beta from amyloid PET images

Arina A. Tagmazian¹  | Claudia Schwarz^{1,2}  | Catharina Lange³  |
Esa Pitkänen¹  | Eero Vuoksima¹  |
for the Alzheimer's Disease Neuroimaging Initiative

¹Institute for Molecular Medicine Finland (FIMM), HiLIFE, University of Helsinki, Helsinki, Finland

²Department of Neurology, University Medicine Greifswald, Greifswald, Germany

³Department of Nuclear Medicine, Charité - Universitätsmedizin Berlin, Corporate Member of Freie Universität Berlin and Humboldt-Universität zu Berlin, Berlin, Germany

Correspondence

Eero Vuoksima and Esa Pitkänen, Institute for Molecular Medicine Finland (FIMM), HiLIFE, University of Helsinki, Helsinki, Finland.
Email: eero.vuoksima@helsinki.fi; esa.pitkanen@helsinki.fi

Funding information

Alzheimer's Disease Neuroimaging Initiative; Doctoral Programme in

Abstract

Detection and measurement of amyloid-beta (A β) in the brain is a key factor for early identification and diagnosis of Alzheimer's disease (AD). We aimed to develop a deep learning model to predict A β cerebrospinal fluid (CSF) concentration directly from amyloid PET images, independent of tracers, brain reference regions or preselected regions of interest. We used 1870 A β PET images and CSF measurements to train and validate a convolutional neural network ("ArcheD"). We evaluated the ArcheD performance in relation to episodic memory and the standardized uptake value ratio (SUVR) of cortical A β . We also compared the brain region's relevance for the model's CSF prediction within clinical-based and biological-based classifications. ArcheD-predicted A β CSF values correlated with measured A β CSF values ($r = 0.92$; $q < 0.01$), SUVR ($r_{AV45} = -0.64$, $r_{FBB} = -0.69$; $q < 0.01$) and episodic memory measures ($0.33 < r < 0.44$; $q < 0.01$). For both classifications, cerebral white matter significantly contributed to CSF prediction ($q < 0.01$), specifically in non-symptomatic and early stages of AD. However, in late-stage disease, the brain stem, subcortical areas, cortical lobes, limbic lobe and basal forebrain made

List of abbreviations: A (A+;A-), Amyloid-beta (amyloid positive and negative CSF measurements based on cut-off values); AD, Alzheimer's disease; ADNI, Alzheimer's Disease Neuroimaging Initiative; aMCI, Amnesic mild cognitive impairment; AV45, Florbetapir; AVLT, Rey Auditory Verbal Learning Test; AVLTdel, Delayed free recall of AVLT; A β , Amyloid-beta; CDR, Clinical dementia rating; CI, Confidence interval; CN, Cognitively normal; CSF, Cerebrospinal fluid; DL, Deep learning; EMCI, Early mild cognitive impairment; FBB, Florbetaben; FDR, False discovery rate; GM, Grey matter; GPU, Graphics processing unit; LM, Logical Memory II of the Wechsler Memory Scale-Revised; LMCI, Late mild cognitive impairment; LMD, Delayed free recall of the LM; LMI, Immediate free recall of the LM; MCI, Mild cognitive impairment; MMSE, Mini-Mental State Examination; MRI, Magnetic resonance imaging; MSE, Mean squared error; PET, Positron emission tomography; r , Correlation coefficient; R^2 , Coefficient of determination; ReLU, Rectified linear activation function; ROI, Region-of-interest; SD, Standard deviation; SMC, Subjective memory complaints; SUVR, Standardized uptake value ratio; T(T+;T-), Tau-related pathology (tau protein-positive and negative CSF measurements based on cut-off values).

Esa Pitkänen and Eero Vuoksima contributed equally

Data used in preparation of this article were obtained from the Alzheimer's Disease Neuroimaging Initiative (ADNI) database (adni.loni.usc.edu). As such, the investigators within the ADNI contributed to the design and implementation of ADNI and/or provided data but did not participate in the analysis or writing of this report. A complete listing of ADNI investigators can be found at: http://adni.loni.usc.edu/wp-content/uploads/how_to_apply/ADNI_Acknowledgement_List.pdf

This is an open access article under the terms of the [Creative Commons Attribution](https://creativecommons.org/licenses/by/4.0/) License, which permits use, distribution and reproduction in any medium, provided the original work is properly cited.

© 2024 The Authors. *European Journal of Neuroscience* published by Federation of European Neuroscience Societies and John Wiley & Sons Ltd.

Population Health of the University of Helsinki (AT); Academy of Finland, Grant/Award Numbers: 314639, 320109, 345988, 322675, 328890; National Institutes of Health, Grant/Award Number: U01 AG024904; Department of Defense, Grant/Award Number: W81XWH-12-2-0012; National Institute on Aging; National Institute of Biomedical Imaging and Bioengineering; Canadian Institutes of Health Research

Edited by: Yoland Smith

more significant contributions ($q < 0.01$). Considering cortical grey matter separately, the parietal lobe was the strongest predictor of CSF amyloid levels in those with prodromal or early AD, while the temporal lobe played a more crucial role for those with AD. In summary, ArcheD reliably predicted A β CSF concentration from A β PET scans, offering potential clinical utility for A β level determination.

KEYWORDS

Alzheimer's disease, amyloid, cerebrospinal fluid, deep learning, PET

1 | INTRODUCTION

Early detection and diagnosis of Alzheimer's disease (AD) can help in the prevention of dementia and in identifying at-risk individuals for clinical drug or lifestyle intervention trials. Even though AD is characterized by both clinical symptoms and neuropathological changes, diagnostic guidelines have been based on clinical symptoms, in particular on episodic memory impairment (Jack et al., 2011; McKhann et al., 1984). However, clinical classification based on symptoms is neither sensitive nor specific for AD, as cognitive impairment can be caused by other neurodegenerative diseases or other reasons (Erickson et al., 2022; Jack et al., 2018; Sperling et al., 2013). Approximately 10–30% of those with clinically defined AD do not have AD-specific neuropathological changes of amyloid-beta (A β) plaques and neurofibrillary tangles of hyperphosphorylated tau on autopsy (Nelson et al., 2011). Moreover, about 30% of cognitively healthy individuals have substantial AD-related neuropathological changes (Aizenstein et al., 2008; Knopman et al., 2003).

Acknowledging the inconsistency between cognitive status and AD-related brain pathology, the biological classification of AD is based solely on biomarkers and defines AD independently of the cognitive status (Jack et al., 2011). The AT(N) framework – and its extension ATX(N) – are based on biological hallmarks of AD: A β (A), tau (T) related pathology and also neurodegeneration (N) (Jack et al., 2018) and potential novel biomarkers (X) (Hampel, Cummings, et al., 2021). Aggregation of A β can start even decades before the onset of the first clinical symptoms, whereas tau protein deposition begins much later and closer to the first clinical symptoms (Jack et al., 2010). Based on A β and tau measurements in cerebrospinal fluid (CSF) and positron emission tomography (PET) and determination of neurodegeneration via PET or magnetic resonance imaging (MRI) scans, the AT(N) framework yields eight biomarker profiles, which separate the AD continuum from non-AD pathologic

changes and normal AD biomarkers (Jack et al., 2018). In the biological framework, it is the A β positivity that is needed to define an individual on the Alzheimer's continuum (Jack et al., 2018). Further, cognitive status is evaluated independently of the biomarker profile and is used for disease staging. Although biomarkers are currently supplementary in clinical practice of AD definition (Arias et al., 2024; Ashton et al., 2024; Jack et al., 2018) and/or limited to memory clinics, biological classification is intended to improve the definition, classification and diagnosis of AD as a unique neurodegenerative disease (Hampel et al., 2022).

Large neuroimaging datasets with PET measurements of AD biomarkers provide an excellent opportunity to further evaluate the AT(N) framework (Weber et al., 2021). Deep learning (DL) models have shown high accuracy in classifying AD and its progression from MRI and PET images (Jo et al., 2019). The majority of the models have used MRI or PET scans to predict clinical disease stages, early disease detection or disease progression (Choi et al., 2020; Ding et al., 2019; Jo et al., 2020; Lin et al., 2021). Only a few studies have aimed to predict AD with amyloid biomarkers (Kim et al., 2019; Reith et al., 2020, 2021). However, these models were trained to quantify the standardized uptake value ratios (SUVR), to classify amyloid status and to predict a change in amyloid pathology on future scans. So far, models have not been trained to predict continuous A β (based on CSF) from the amyloid PET (independent of the A β tracer type, preselected regions of interest, brain reference region and SUVR definition) (Palmqvist et al., 2015; Spallazzi et al., 2019). Such a prediction studies the link between the localization of amyloid in the brain and CSF amyloid levels across the entire continuum of biomarker aggregation. In the case PET imaging is done in clinical practice, ArcheD would allow using only one biomarker, thus decreasing clinicians' workload, avoiding invasive CSF sampling and following challenging CSF measurement standardization.

In this study, we propose a convolutional neural network model ("ArcheD") with residual connections to

predict A β CSF concentration from amyloid PET images. Residual deep networks have been used in PET image analyses previously (Shah et al., 2022), but here we aimed to assess their applicability in predicting fluid biomarker levels from PET images. Our approach allows probing the model and input amyloid PET images to reveal the brain regions that contribute most to the predicted CSF amyloid concentrations. ArcheD does not use any prespecified cortical (or other) brain regions, but instead adopts a hypothesis-free approach leveraging all information available in PET images. To examine our approach, we compared our method's performance with SUVR, a measure that determines cortical amyloid aggregation in relation to the cerebellum, a commonly used reference region (Heeman et al., 2020; Jack et al., 2013). We also studied our model in relation to episodic memory including immediate and delayed recall measures. We further investigated the model and brain regions separately in sub-groups based on both clinical and biological classification of AD. To scrutinize the trained neural network model, we extracted brain regions that the model considers informative for CSF prediction and compared them between clinical and biological classes.

2 | METHODS AND MATERIALS

2.1 | Data and participants

We studied 1252 individuals' PET data on brain amyloid and CSF measurements of amyloid- β 1–42 peptide and phosphorylated tau 181P provided by the Alzheimer's Disease Neuroimaging Initiative (ADNI).

Data used in the preparation of this article were obtained from the Alzheimer's Disease Neuroimaging Initiative (ADNI) database (adni.loni.usc.edu). The ADNI was launched in 2003 as a public-private partnership, led by Principal Investigator Michael W. Weiner, MD. The primary goal of ADNI has been to test whether serial magnetic resonance imaging (MRI), positron emission tomography (PET), other biological markers and clinical and neuropsychological assessment can be combined to measure the progression of mild cognitive impairment (MCI) and early Alzheimer's disease (AD). For up-to-date information, see <https://adni.loni.usc.edu/>. (Petersen et al., 2010).

We used PET and MRI scans, CSF measurements, ADNI clinical classifications, episodic memory measurements and demographics data (adni.loni.usc.edu). Amyloid PET scans were obtained with different tracers (i.e., Pittsburgh compound B, Florbetapir, Florbetaben) depending on the ADNI study phase, and pre-processed by the ADNI PET imaging corelab (i.e., 'co-reg, avg,

standardized image and voxel size'). In addition to imaging data, we used the cortical composite standardized uptake value ratios (SUVR) (Kinahan & Fletcher, 2010; Landau et al., 2015) normalized by the whole cerebellum as a reference region, and added it as a standard amyloid measurement from PET in our model's performance evaluation.

As some participants had several clinical visits, a total of 1870 amyloid PET images were obtained. Among them individuals had AD (n = 190), amnesic mild cognitive impairment (aMCI) due to AD (n = 928), subjective memory complaints (SMC) (n = 145) or were cognitively normal (CN) (n = 607) based on the ADNI clinical classification (Table S2). The clinical classifications in ADNI are based on the Clinical Dementia Rating (CDR), the Mini-Mental State Examination (MMSE) and delayed recall of 1 paragraph from the Logical Memory (LM) II of the Wechsler Memory Scale-Revised (Petersen et al., 2010). In addition to clinical classifications, we used immediate and delayed recall measures from the LM Story A and also immediate (total words in trials 1–5) and delayed recall measures of the Rey Auditory Verbal Learning Test (AVLT): these tests were used as continuous measures of episodic memory.

2.2 | Biological classification based on CSF measurements

The biological classes were defined based on earlier established cut-off values of amyloid- β 1–42 and phosphorylated tau CSF measurement (Shaw & Trojanowski, 2017). In the first phases of ADNI, CSF quantification was implemented by INNO-BIA AlzBio3 immunoassay kit-based reagents, however, later the approach was replaced by fully automated Roche Elecsys. These methods have different scaling ranges, consequently, threshold values for biomarker aggregation also differ (amyloid- β : 192 pg/ml for INNO-BIA AlzBio3, 980 pg/ml for Roche Elecsys; tau: 93 pg/ml for INNO-BIA AlzBio3, 245 pg/ml for Roche Elecsys; phosphorylated tau [p-tau]: 23 pg/ml for INNO-BIA AlzBio3, 21.8 pg/ml for Roche Elecsys) (Shaw et al., 2009; Shaw & Trojanowski, 2017).

As a result, we obtained four biological classes: participants with negative amyloid and tau proteins' CSF measurements based on cut-off values (A-T-); amyloid negative, tau positive group (A-T+); amyloid positive, tau negative group (A + T-); amyloid and tau positive group (A + T+). We used only A and T in our biological classification, whereas the neurodegeneration (N) component was not included because it is not currently needed for the biological classification of AD-related pathology (Jack et al., 2018).

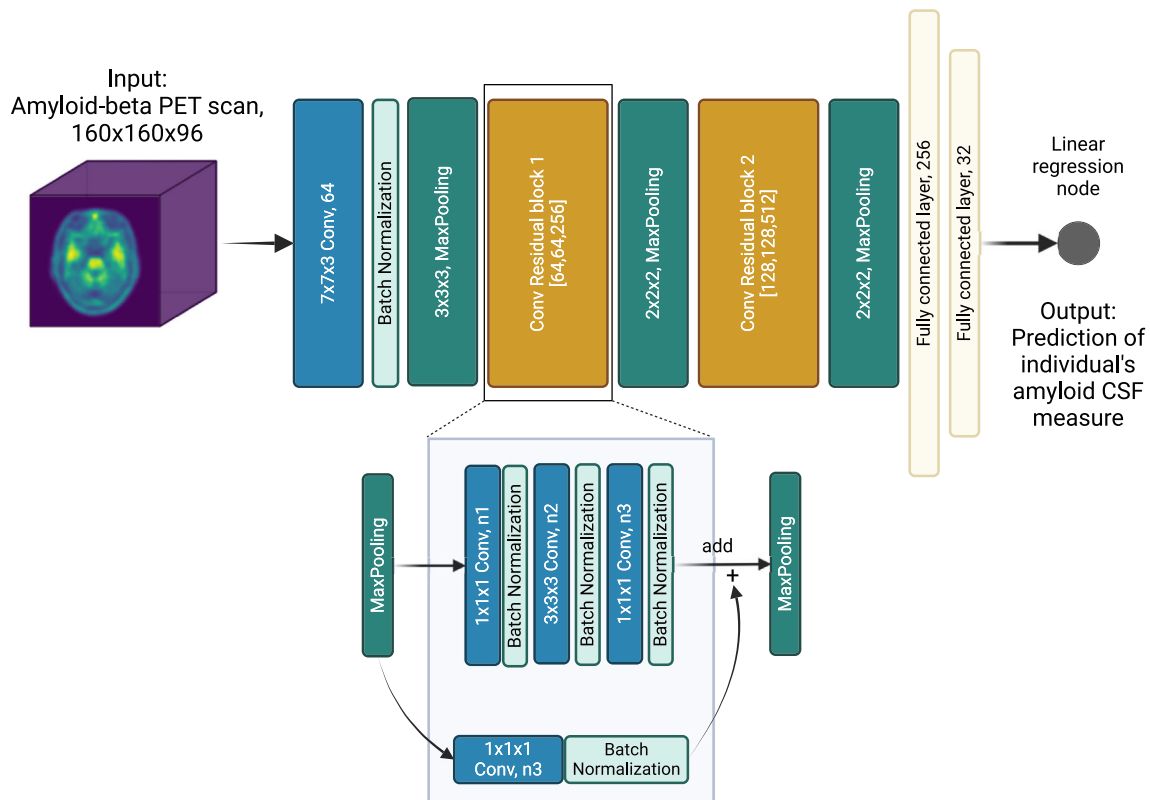


FIGURE 1 Schematic presentation of the ArcheD model architecture. PET – positron emission tomography; CSF – cerebrospinal fluid; n1, n2 and n3 – the number of filters in convolution layers are specified in brackets for both convolutional residual blocks. Created with [BioRender.com](https://www.biorender.com).

2.3 | Fluid biomarker rescaling

To integrate values from the different CSF measurement methods, we trained linear regression and third-degree polynomial regression models to rescale AlzBio3 values to Roche Elecsys based on 1072 samples with both values available (858 training samples, 214 test samples). The model that maximized the coefficient of determination (R^2) and accuracy of positive and negative amyloid classification using cut-off values in the test dataset was selected for further analysis.

2.4 | A deep neural network model to predict CSF values from PET scans

We developed a deep convolutional neural network model called “ArcheD”, which utilizes residual connections (He et al., 2016) to predict logarithmic A β CSF values from amyloid PET scans. The residual connections allow for a deeper model to be trained, which has been shown to improve performance (He et al., 2016). Our model architecture includes one initial convolution-

pooling block followed by two residual-pooling blocks, two fully connected layers and a linear regression node (Figure 1). Each residual block contains a sequence of convolutional, batch normalization and rectified linear activation function (ReLU) activation layers.

ArcheD contains 35 layers and approximately 10.7 millions parameters. To train the model, we used the Adam optimization algorithm (Kingma & Ba, 2014) with an initial learning rate of 0.0001 to minimize the mean squared error (MSE) of observed and predicted CSF values. The model was trained for a maximum of 150 epochs with a minibatch size of four, and stopped early if loss in the validation dataset did not decrease for 15 epochs.

We used 60% of the dataset for training ($n = 1197$), 20% for validation ($n = 299$) and 20% for testing the model ($n = 374$). To increase the size of the training dataset with data augmentation, we either applied Gaussian noise ($\sigma = 0.5, 10, 15, 20, 25\%$; six possible augmentations) or flipped the image by X or Y axes (two possible augmentations). To generate an augmented image from a training dataset image, one of the eight possible augmentations was selected with an equal probability. In the

end, we obtained a total of 14,352 original and augmented brain scans constituting the augmented training data. To evaluate the robustness of ArcheD in data not used in training, we used a test dataset. ArcheD code is available at GITHUB (<https://github.com/artagmaz/arched.git>).

2.5 | Guided backpropagation relevance maps

To explore which brain regions contribute the most to ArcheD's predictions of amyloid CSF measurements from amyloid PET scans, we used the guided backpropagation technique (Springenberg et al., 2014). This approach quantifies how much model outputs change in response to perturbing model inputs. In PET imaging data, we used guided backpropagation to extract the contribution (relevance value) of each input voxel to CSF prediction. Guided backpropagation creates more specific relevance value maps compared to the classic backpropagation approach by replacing negative gradients with zero in ReLU activation layers during backward passes (Rieke et al., 2018) (Figure 2.1).

To compare the relevance maps between individuals and AD classes, we co-registered PET scans and corresponding relevance maps to individuals' MRI and MNI152 templates with the AntsPy package (Avants et al., 2009) (Figure 2.2). Since all PET images and relevance maps were described in the same coordinate space, we were able to create average PET and relevance maps for all samples and separate AD classes. We used the neuroinformatics atlas to derive regions-of-interest (ROIs) (Bakker et al., 2015) (Table S1, Figure 2.3) and compared their relevance to the model decision-making between classes (Figure 2.4). The relevance value per ROI was normalized to the size of the region to evaluate

how relevant the average voxel of each area is for CSF predictions.

2.6 | Statistical analyses

We computed Pearson correlations with two-tailed p-values to quantify the strength of the associations between model prediction and CSF A β , cortical SUVR and episodic memory measures. We also compared relevance values of brain areas between biological or clinical classes by bootstrapping with a 95% confidence interval, Cohen's *d* and Welch's t-test. For all multiple comparisons, we computed false discovery rates (FDR) with the Benjamini-Hochberg method.

2.7 | Programming environment

Tensorflow 2.4.1 and Python 3.9.7 were used to develop the machine-learning models and perform computational analyses. The models were trained on NVIDIA Tesla V100 GPUs with 16 GB memory. For uploading, augmentation, registration and visualization of PET images we used nibabel, dltk and AntsPy python packages (Avants et al., 2009; Brett et al., 2023; Pawlowski et al., 2017). Functions for guided backpropagation gradient analysis were adapted from <https://github.com/jrieke/cnn-interpretability>. All R and Python scripts used in the study are provided at <https://github.com/artagmaz/arched.git>.

3 | RESULTS

The mean age of the participants was 73.6 years (SD = 7.37) and 49% were women. Detailed descriptive statistics of study participants are presented in Table S2.

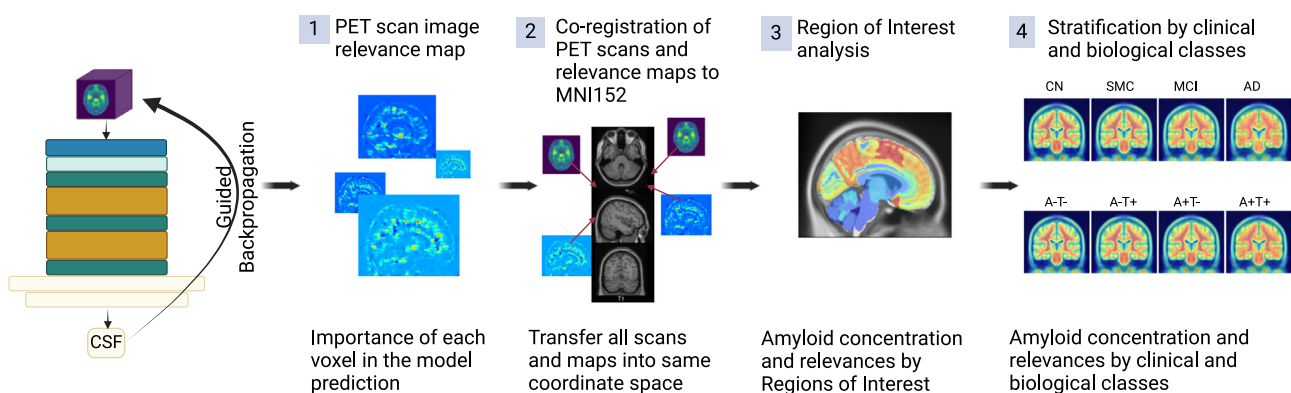


FIGURE 2 Workflow to process PET scans with ArcheD and guided backpropagation to identify characteristics distinguishing brain regions of interest and clinical and biological groups. Created with BioRender.com.

3.1 | Model training

3.1.1 | Fluid biomarker rescaling

We first transformed AlzBio3 CSF values to conform to the range of values present in Roche Elecsys CSF

measurements (Shaw & Trojanowski, 2017). Both regression models performed similarly on a held-out portion of the data (linear regression: $R^2_{\text{test}} = 68.9\%$, 91.5% accuracy; third-degree polynomial regression: $R^2_{\text{test}} = 69.4\%$, 91.5% accuracy) (Table S3, Figure S1). Based on these metrics and visual inspection of the regression models

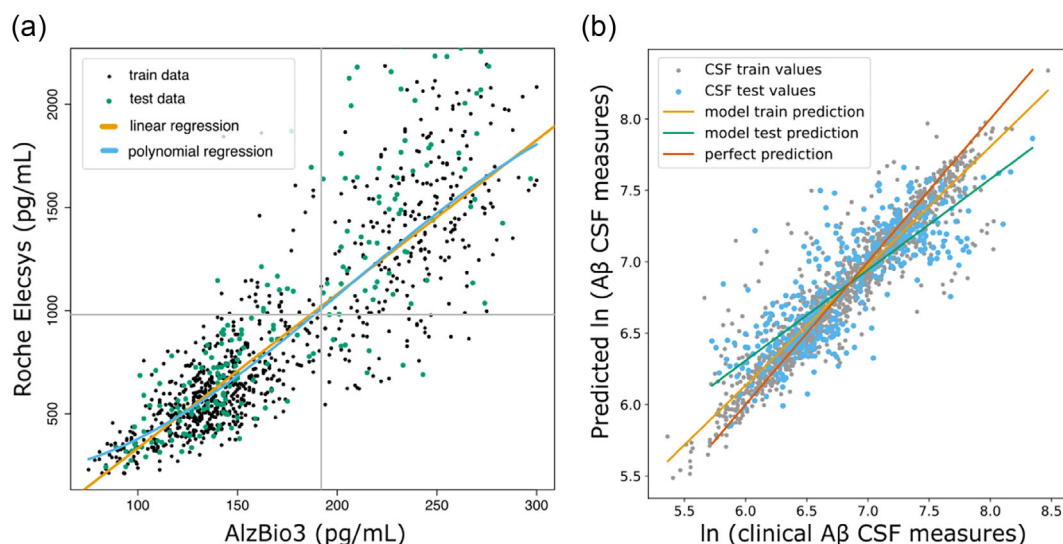


FIGURE 3 (a) Linear (orange line) and third-degree polynomial (blue line) regression for fluid amyloid rescaling from INNO-BIA AlzBio3 system to Roche Elecsys. Grey lines present cut-off values for Aβ CSF measurement. (b) Comparison of clinically measured Aβ CSF and values predicted by the ArcheD model. CSF values are given as natural logarithms. Lines illustrate the linear relationship between clinical Aβ CSF measurement and prediction of our model: green – linear relation between real and predicted values of the test dataset; orange – linear relation between real and predicted values of the training dataset. The red diagonal line shows the ideal one-to-one correspondence between observed and predicted values.

TABLE 1 Pearson correlations between Aβ CSF values predicted by model and clinical, imaging and memory markers of AD.

	Clinical Aβ CSF	SUVr (AV45/FBB)	LMI	LMD	AVLT 1-5	AVLTdel
Clinical Aβ CSF (all samples, 1870)	1.0**	-0.64**/ -0.66**	0.46**	0.45**	0.38**	0.32**
SUVr AV45 (all samples, 883)	-0.64**	1.0**	-0.40**	-0.40**	-0.36**	-0.31**
Predicted Aβ CSF (all samples, 1870)	0.92**	-0.64**/ -0.69**	0.44**	0.44**	0.38**	0.33**
AD (190)	0.89**	-0.42*/ -0.08	-0.09	-0.02	0.36**	0.20
MCI (928)	0.91**	-0.66**/ -0.75**	0.43**	0.42**	0.32**	0.28**
LMCI (259)	0.90**	-0.53**/NA	0.42**	0.44**	0.34**	0.32**
EMCI (449)	0.92**	-0.68**/NA	0.38**	0.36**	0.28**	0.24**
SMC (145)	0.89**	-0.75**/NA	0.12	0.09	0.05	0.25
CN (607)	0.90**	-0.53**/ -0.63**	0.24**	0.26**	0.21**	0.16**

*FDR < 5%.

**FDR < 1%, FDR correction was performed across all tests.

Abbreviation: SUVr – standardized uptake value ratio; AV45 and FBB – Aβ tracers; LMI – immediate free recall of Logical Memory (LM) II Story A of the Wechsler Memory Scale; LMD – delayed free recall of the LM; AVLT 1-5 – total number of words in trials 1-5 of the Rey Auditory Verbal Learning Test (AVLT); AVLTdel – delayed free recall of AVLT. NA indicates categories with no samples to test.

(Figure 3a), we decided to use a third-degree polynomial regression model to predict Roche Elecsys amyloid measurements for the remaining 1102 samples.

3.1.2 | Training the ArcheD model and overall predictive performance

ArcheD was trained on 14,352 augmented PET scan images to predict logarithmic CSF values. The model achieving the best performance in the validation set was obtained after the eighth epoch of training (mean squared error, MSE = 0.12) (Figure S1). Finally, ArcheD explained 66% of the variance (R^2) in the test dataset not used in training (Figure 3b).

3.2 | Associations of DL with SUVR and episodic memory measurements

The ArcheD A β CSF prediction was correlated with biological and cognitive AD markers (Table 1). A significant association was observed between predicted and clinically measured CSF A β , both for all samples and all clinical classes ($r > 0.89$, $q < 0.01$). SUVR strongly correlated with all sample subsets' A β CSF ($r < -0.53$, $q < 0.01$) except for AD samples ($r_{AV45} = -0.42$, $q < 0.05$; $r_{FBB} = -0.08$, $q = 0.76$). In the case of episodic memory test results, CSF predictions were generally weaker and mostly non-significant in the AD ($n = 190$) and SMC ($n = 145$) groups compared to MCI ($n = 928$) and CN ($n = 607$) groups. There was a significant positive correlation in AD samples between predicted A β CSF and AVLT immediate recall ($r = 0.36$; $q < 0.01$), whereas in those with SMC predicted CSF measurements showed no significant correlations with any of the episodic memory measures (Table 1). All memory test scores for MCI and CN groups were significantly correlated with predicted amyloid CSF measurement ($r > 0.16$, $q < 0.01$) (Table 1).

3.3 | Relevance of brain areas for model decision-making

To understand which brain regions contributed the most to ArcheD predictions, we compared the relevance of these regions with guided backpropagation. We found that the areas that contributed the most were cerebral (mean relevance 0.251, 95% CI [0.247, 0.255]) and cerebellum white matter (0.207, 95% CI [0.205;0.208]) followed by the brain stem, subcortical areas, grey matter regions at the lobar level and cerebellum grey matter,

whereas limbic lobe, basal forebrain, ventricles and optic chiasm were substantially less important for the model (Table S4, Figure 4a,b).

We then explored the clustering of ROIs in the ADNI cohort by examining their similarity based on relevance profiles (Figure 4c). This analysis aimed to enhance our understanding of the region-specific contributions to our model. As expected, cerebral and cerebellum white matter, and vessels clustered together. The main cerebral lobes, i.e., frontal, temporal, parietal and occipital lobes were clustered together, as were the brainstem and subcortical regions. The remaining regions formed two clusters containing optic chiasm and ventricles, and basal forebrain and limbic lobe (Figure 4c).

3.4 | Region-specific contributions to prediction of CSF in clinical and biological sub-classes

Different brain regions may have different levels of contribution to the model's prediction of CSF values. These differences may also vary as a function of the stage in the AD continuum. Therefore, we compared their relevance values within both clinical (CN, SMC, MCI, AD) and biological (A-T-, A-T+, A + T-, A + T+) classifications. The between-classes analysis showed that there were brain areas that contributed at the same level for all clinical or biological classes (optic chiasm, ventricles and vessels) and areas that were significantly different between classes by relevance value (Figure S3, Figure 5, Table S4).

Significant differences in relevance values between AD/MCI and CN groups were observed in eight ROIs ($q < 0.01$) (Table S5). Cerebral white matter contributed more to A β CSF value predictions in the CN group (AD vs CN Cohen's $d = -0.976$, A + T + vs A-T- $d = -1.138$; $q < 0.01$), whereas other regions (cortical lobes, limbic lobe, basal forebrain and subcortical areas) were more important for prediction in the AD and MCI groups (Table S5). Brainstem relevance values differentiated only between MCI and CN groups (Figure 5, Table S5). However, there were no significant differences between SMC and CN groups (Figure 5, Table S5).

Most of the relevance patterns observed for biological classes were concordant with those seen in clinical classes. In all ROIs, except vessels, ventricles and optic chiasm, a marked difference in relevance values was visible between A + T + and A-T- classes (Figure 5, Table S5). In addition, parietal, occipital, frontal, temporal lobes, brain stem, cerebral white matter and subcortical areas differentiated A + T- from the A-T- ($q < 0.01$) (Figure 5, Table S5).

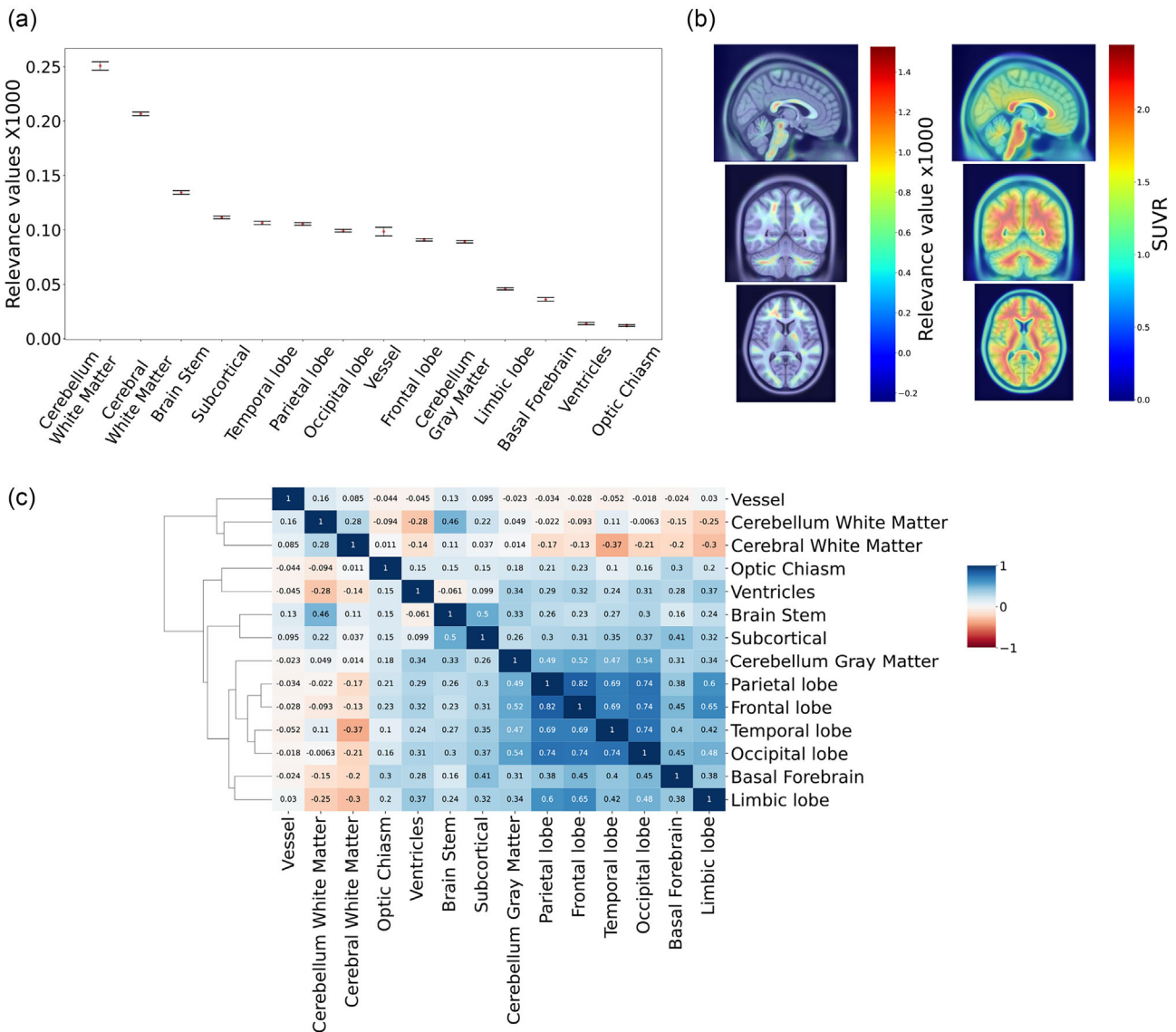


FIGURE 4 (a) Mean relevance values for brain regions and bootstrapped 95% confidence intervals. Values were multiplied by 1000. (b) Average relevance value and amyloid concentration (SUVR) for the dataset on PET scan. (c) Heatmap of Pearson correlations for relevance values of all brain regions.

3.5 | Contribution of grey matter regions to Aβ CSF prediction in clinical and biological classes

Taking into account the high amount of unspecified binding of the amyloid tracers in cerebral and cerebellar white matter, we conducted a closer investigation focusing only on the cortical grey matter (GM) regions (Figure 4b) (Klunk et al., 2004). GM regions are first affected by the neuropathological changes of AD (Thal et al., 2002) and our results indicated that these regions contributed more to the model prediction of later stages of the disease (Figure 5). Therefore, we explored their

contribution to AD development in clinical and biological classes.

At the lobar level, temporal (mean relevance 0.106, 95% CI [0.105, 0.108]) and parietal (0.105, 95% CI [0.104, 0.107]) lobes contributed the most to the model prediction. In contrast, occipital (0.098, 95% CI [0.098, 0.100]) and frontal lobes (0.091, 95% CI [0.089, 0.92]) had significantly lower relevance values than temporal and parietal lobes (Figure 6a). However, when looking at absolute levels of PET amyloid binding as expressed by SUVR, parietal (mean SUVR 1.449, 95% CI [1.432, 1.466]), occipital (mean 1.440, 95% CI [1.426, 1.455]) and frontal (1.435, 95% CI [1.419, 1.452]) lobes showed higher levels

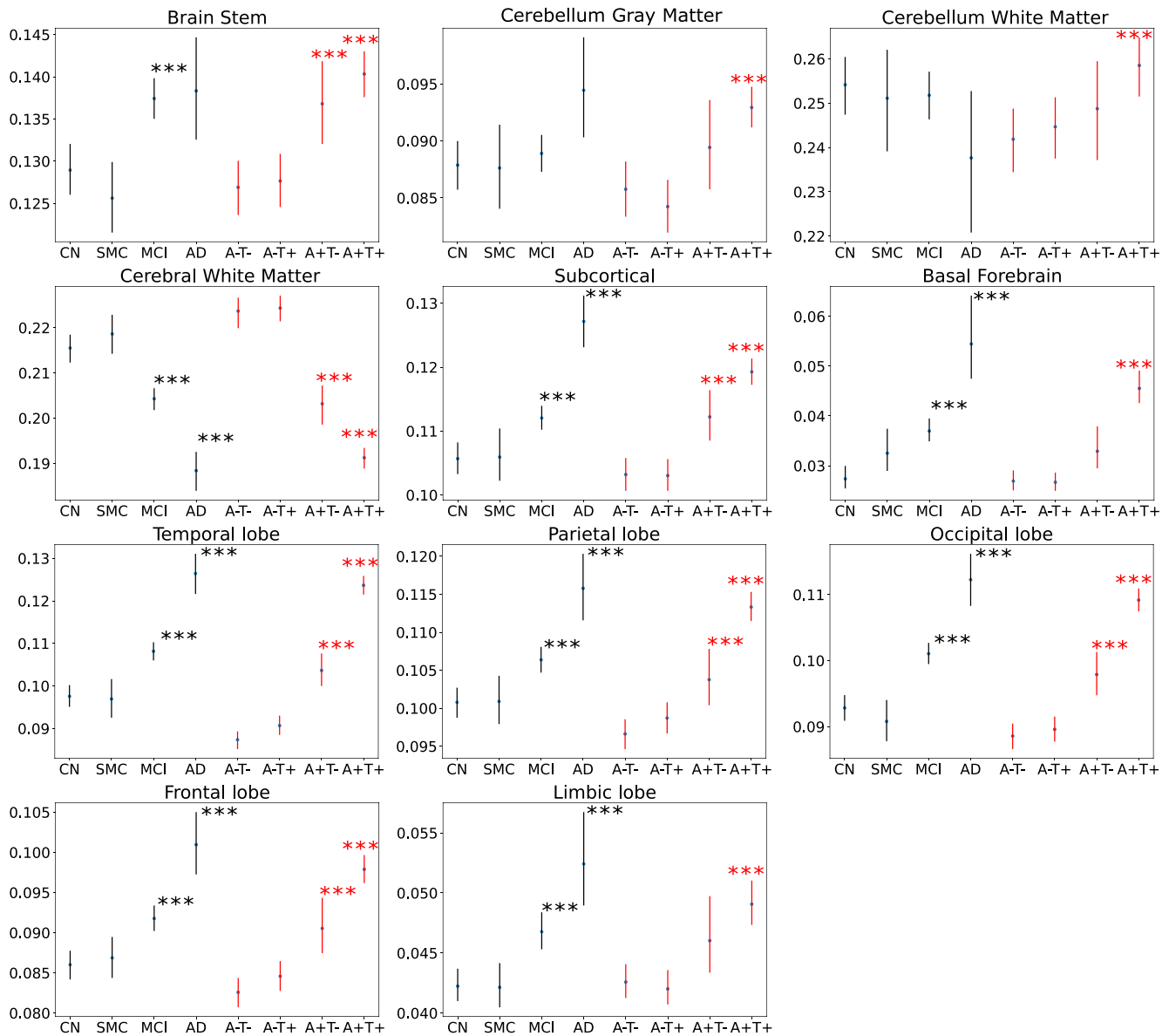


FIGURE 5 Comparison of mean relevance values per brain region within clinical or biological classifications. The cognitive normal (CN) group was used as a control for clinical classification. A-T- was used as a control for biological classification. *** - $q < 0.01$.

of amyloid aggregation compared to the temporal lobe (1.359, 95% CI [1.344, 1.375]) (Figure 6a).

When comparing relevance value differences between biological or clinical classes, we observed that the most contributing grey matter region differed along the AD continuum (Figure 6b, Table S6). In the CN and SMC groups (based on the clinical classification), the parietal lobe (CN mean 0.101, 95% CI [0.099, 0.103]; SMC 0.101, 95% CI [0.098, 0.104]) was the most significantly contributing region, followed by the temporal, occipital lobes, cerebellum grey matter and frontal lobe (Figure 6b, Table S6). In MCI and AD groups, the relevance values of all regions were higher than in the CN group, and the temporal lobe contributed more than the other lobes

(MCI temporal 0.108, 95% CI [0.106, 0.110]; AD temporal 0.126, 95% CI [0.122, 0.131]).

For biological classification, we observed a similar pattern in terms of the early versus late stages of the AD continuum. In the A-T- group, the parietal lobe (0.097, 95% CI [0.095, 0.098]) contributed most significantly to the model decision-making, followed by the occipital, temporal lobes, cerebellum grey matter and frontal lobe (Figure 6b, Table S6). In the A-T+ and A+T- groups, the temporal lobe was more relevant than occipital area (A-T+ temporal 0.091, 95% CI [0.089, 0.093]; A+T- temporal 0.104, 95% CI [0.100, 0.108]), and dominated all other grey matter regions in A+T+ class (0.124, 95% CI [0.122, 0.126]) (Figure 6b, Table S6).

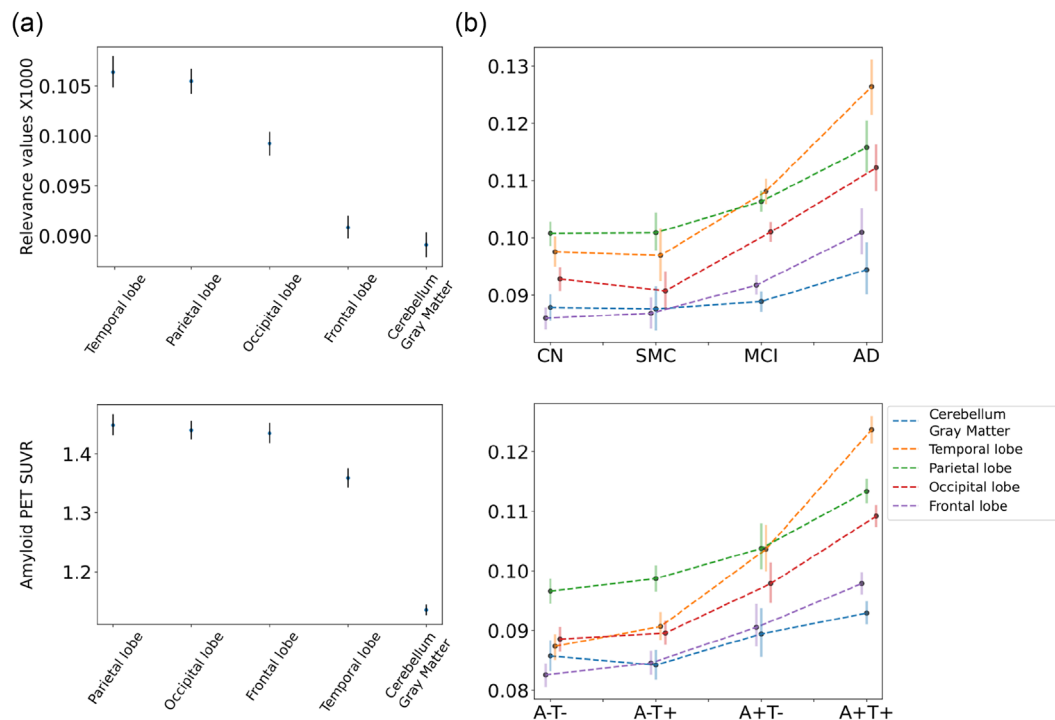


FIGURE 6 (a) Mean relevance values (top) and amyloid concentration (bottom) for grey matter regions and bootstrapped 95% confidence intervals. (b) Relevance level of grey matter regions on different clinical (top) and biological classes (bottom) of AD.

4 | DISCUSSION

We developed a deep neural network model (ArcheD) for the prediction of CSF amyloid biomarker concentration directly from amyloid PET images independent of the amyloid PET tracer. Trained on ADNI PET images and associated A β CSF measurements, ArcheD was able to explain 66% of the variance in CSF levels in a test dataset withheld from training. We thus envision using ArcheD to complement the information obtained in an A β PET scan by providing an estimate of the A β CSF level without a lumbar puncture.

CSF A β predicted by our model correlated significantly with cortical amyloid PET SUVR and episodic memory performance. The correlations of measured and predicted A β CSF with PET SUVR and episodic memory measurements were highly similar (Hake et al., 2015; Niemantsverdriet et al., 2017) and can be interpreted as additional proof of the model's prediction accuracy. The absence of association in AD and SMC groups with FBB SUVR and episodic memory performance could be explained by the smaller number of participants in these classes compared to group sizes of CN and MCI. In addition, the AD group included individuals with severe AD, resulting in little variation in amyloid levels and episodic memory performance; amyloid levels plateau in the

course of AD and there is also little variation in delayed recall measures in those with severe AD (Klunk et al., 2004; Thal et al., 2002).

To understand which brain regions were the most influential in predicting CSF A β levels, we investigated the relevance of average voxel per brain region and compared ROIs between each other, and, furthermore, performed these comparisons separately in clinical and biological sub-classes. The cerebellum and cerebral white matter, followed by the subcortical area and brainstem, were identified as the most influential brain regions for model predictions. Some of these regions have unspecific binding of amyloid tracers (Klunk et al., 2004; Matsubara et al., 2016) and can be used as visual control regions to test the tracers' delivery to the brain. They are also not affected by amyloid plaques until the very late AD stage (Klunk et al., 2004; Thal et al., 2002) and can be used as possible reference regions for calculating SUVR (Heeman et al., 2020), even if cerebellum grey and white matter is the gold standard reference region (Klunk et al., 2015). It is likely that our ArcheD model learnt to use these regions as a reference point for CSF prediction and combined them with cortical regions to 'calibrate' amyloid CSF values. Furthermore, supporting evidence comes from the clustering of ROIs based on their relevance profiles (Figure 4c). This clustering distinctly separated

white matter and vessels from other brain regions and effectively grouped all grey matter regions and cerebellum grey matter together.

Areas contributing the least to the model's predictions were the limbic lobe, basal forebrain, ventricles and optic chiasm. Despite hippocampus and basal forebrain degeneration being characteristic of early-stage AD (Hampel, Hardy, et al., 2021; Kerbler et al., 2015; Teipel et al., 2018), ArcheD did not consider them informative for CSF prediction. This can be attributed to the small size of these ROIs and the limited spatial resolution of PET scans, resulting in a partial-volume effect (Soret et al., 2007).

Furthermore, we explored whether the same or different regions contributed to CSF prediction in different clinical and biological classes. Relevance of cerebral cortex (including limbic lobe), subcortical, brain stem, basal forebrain, cerebellum white and grey matter regions was significantly greater in those with AD compared to those without AD or in those who were amyloid positive compared to those who were amyloid negative. Cerebral white matter contributed more to CSF prediction in individuals without cognitive impairment (CN, SMC) or in individuals who were amyloid negative (A-T-, A-T+). According to criteria for amyloid PET scan usage, amyloid-positive scans differentiate from amyloid-negative scans based on grey matter cortical uptake that is above the level of nonspecific binding in white matter (Johnson et al., 2013; Richards & Sabbagh, 2014; Wolk et al., 2012). This corresponds to our finding, indicating that cerebral white matter plays a more significant role in CSF prediction for amyloid-negative groups, while cortical regions are more relevant to amyloid-positive individuals. We hypothesized that ArcheD might not only use cerebral white matter as a reference region but also focus on both white and grey matter amyloid binding levels together.

Focusing on cortical GM, we found considerable differences between lobes' relevance values and amyloid deposition level. Temporal and parietal areas contributed the most to the model prediction, whereas occipital and frontal lobes' relevance values were noticeably less. The temporal lobe has been reported to substantially contribute to model decision-making also in other studies of AD classification based on MRI scans (Dyrba et al., 2021; Rieke et al., 2018). However, on PET scans, the parietal, occipital and frontal lobes have higher levels of amyloid aggregation, while the temporal lobe has significantly less amyloid. According to the A β pathology studies, parietal and frontal lobes are regions with early amyloid accumulation, which can explain the high biomarker concentration in those regions in our results (Insel et al., 2020; Mattsson et al., 2019).

Despite the temporal lobe being the least amyloid-enriched lobe in PET scans, ArcheD highlighted this lobe as the most important cortical region for the amyloid CSF prediction. When we looked at the level of cortical lobes' relevance between different classes, we noticed that the temporal lobe's relevance is more important than other lobes only in MCI, AD and A + T + groups, which indicate later stages in the AD continuum compared to SMC, CN and A-negative groups. In early stages of the disease development, the parietal lobe is the most significant contributor, which is compatible with earlier studies (Insel et al., 2020; Mattsson et al., 2019).

This study presented a novel neural network model that analyses amyloid PET scans, independent of the amyloid tracer used and predicts what the amyloid beta level would be in CSF. The model learned to focus on specific brain regions depending on the AD stage, defined by the biological or clinical classification. These regions aligned well with previous findings on AD progression.

ArcheD has the potential to be used in clinical practice in the future. It can reduce the amount of work for clinicians and potentially prevent patients from lumbar puncture. ArcheD is also straightforward to use, as the PET scan image is the only input to the method. However, our research has some limitations that can be improved in future studies. We had only a limited dataset of PET scans with available CSF measurements, especially of AD individuals, to train the ArcheD model. Larger training datasets would likely yield better predictive performance. Another limiting factor is the strict requirement for input PET images to have dimensions of 160x160x96 voxels. Therefore, users may need to perform preprocessing, such as co-registration, averaging, standardization and voxel size adjustment, similar to ADNI PET imaging corelab, on their own. Our model and findings also need to be validated on external datasets.

5 | CONCLUSION

In conclusion, ArcheD was able to predict amyloid CSF values directly from amyloid PET scans in the AD continuum (including cognitively unimpaired individuals with preclinical AD). Predicted CSF values correlated significantly with CSF amyloid, cortical amyloid SUVR and episodic memory performance. Analysing the relevance of brain regions to model's CSF prediction, cerebellar and cerebral white matter, brainstem and subcortical areas were found to contribute the most and may have been used by ArcheD as reference regions for prediction. Upon comparing clinical and biological classes we found that the subcortical areas, brain stem, cerebellum, cerebral cortex and its subregion - the basal forebrain, influenced

predictions, especially in the MCI and AD clinical subclasses and A + T- and A + T + biomarker-defined classes. Moreover, cerebral white matter contributed more to clinically normal and biologically defined early-stage groups. Examining cortical regions more closely, we observed a constant higher level of the temporal lobe relevance along the entire AD continuum and assumed that the model prioritized it as a predictor of A β CSF. Our model can serve in clinical practice for determining an A β CSF state and improving AD early detection. However, further studies are needed to validate and tune the model for clinical use.

AUTHOR CONTRIBUTIONS

Arina A. Tagmazian: Conceptualization, Data Curation, Formal Analysis, Investigation, Methodology, Project administration, Software, Visualization, Writing – Original Draft, Writing – Review & Editing.

Claudia Schwarz: Conceptualization, Investigation, Writing – Original Draft Preparation, Writing – Review & Editing.

Catharina Lange: Investigation, Writing – Original Draft Preparation, Writing – Review & Editing.

Esa Pitkänen: Conceptualization, Data curation, Funding Acquisition, Methodology, Investigation, Project administration, Supervision, Writing – Original Draft Preparation, Writing – Review & Editing.

Eero Vuoksima: Conceptualization, Funding Acquisition, Methodology, Investigation, Project administration, Supervision, Writing – Original Draft Preparation, Writing – Review & Editing.

ACKNOWLEDGEMENTS

The authors wish to acknowledge CSC – IT Center for Science, Finland, for generous computational resources.

This study was supported by the Doctoral Programme in Population Health of the University of Helsinki (AT) and the Academy of Finland (grants 314639, 320109 and 345988 to EV and 322675 and 328890 to EP).

Data collection and sharing for this project was funded by the Alzheimer's Disease Neuroimaging Initiative (ADNI) (National Institutes of Health Grant U01 AG024904) and DOD ADNI (Department of Defense award number W81XWH-12-2-0012). ADNI is funded by the National Institute on Aging, the National Institute of Biomedical Imaging and Bioengineering, and through generous contributions from the following: AbbVie, Alzheimer's Association; Alzheimer's Drug Discovery Foundation; Araclon Biotech; BioClinica, Inc.; Biogen; Bristol-Myers Squibb Company; CereSpir, Inc.; Cogstate; Eisai Inc.; Elan Pharmaceuticals, Inc.; Eli Lilly and Company; EuroImmun; F. Hoffmann-La Roche Ltd and its affiliated company Genentech, Inc.; Fujirebio; GE

Healthcare; IXICO Ltd.; Janssen Alzheimer Immunotherapy Research & Development, LLC.; Johnson & Johnson Pharmaceutical Research & Development LLC.; Lumosity; Lundbeck; Merck & Co., Inc.; Meso Scale Diagnostics, LLC.; NeuroRx Research; Neurotrack Technologies; Novartis Pharmaceuticals Corporation; Pfizer Inc.; Piramal Imaging; Servier; Takeda Pharmaceutical Company; and Transition Therapeutics. The Canadian Institutes of Health Research is providing funds to support ADNI clinical sites in Canada. Private sector contributions are facilitated by the Foundation for the National Institutes of Health (www.fnih.org). The grantee organization is the Northern California Institute for Research and Education, and the study is coordinated by the Alzheimer's Therapeutic Research Institute at the University of Southern California. ADNI data are disseminated by the Laboratory for Neuro Imaging at the University of Southern California.

CONFLICT OF INTEREST STATEMENT

The authors have no conflict of interest to declare.

DATA AVAILABILITY STATEMENT

The code and ArcheD model that support the findings of this study are available in Github at <https://github.com/artagmaz/arched.git>.


PEER REVIEW

The peer review history for this article is available at <https://www.webofscience.com/api/gateway/wos/peer-review/10.1111/ejn.16332>.

ORCID

Arina A. Tagmazian  <https://orcid.org/0000-0002-2906-6279>

Claudia Schwarz  <https://orcid.org/0000-0003-3234-912X>

Catharina Lange  <https://orcid.org/0000-0002-6745-8441>

Esa Pitkänen  <https://orcid.org/0000-0002-9818-6370>

Eero Vuoksima  <https://orcid.org/0000-0002-6534-3667>

REFERENCES

- Aizenstein, H. J., Nebes, R. D., Saxton, J. A., Price, J. C., Mathis, C. A., Tsopelas, N. D., Ziolkowski, S. K., James, J. A., Snitz, B. E., Houck, P. R., Bi, W., Cohen, A. D., Lopresti, B. J., DeKosky, S. T., Halligan, E. M., & Klunk, W. E. (2008). Frequent amyloid deposition without significant cognitive impairment among the elderly. *Archives of Neurology*, *65*(11), 1509–1517. <https://doi.org/10.1001/archneur.65.11.1509>
- Arias, J. J., Manchester, M., & Lah, J. (2024). Direct to consumer biomarker testing for Alzheimer disease—Are we ready for the insurance consequences? *JAMA Neurology*, *81*(2), 107–108. <https://doi.org/10.1001/jamaneurol.2023.4811>

- Ashton, N. J., Brum, W. S., Di Molfetta, G., Benedet, A. L., Arslan, B., Jonaitis, E., Langhough, R. E., Cody, K., Wilson, R., Carlsson, C. M., Vanmechelen, E., Montoliu-Gaya, L., Lantero-Rodriguez, J., Rahmouni, N., Tissot, C., Stevenson, J., Servaes, S., Therriault, J., Pascoal, T., ... Zetterberg, H. (2024). Diagnostic accuracy of a plasma phosphorylated tau 217 immunoassay for Alzheimer disease pathology. *JAMA Neurology*, *81*, 255–263. <https://doi.org/10.1001/jamaneurol.2023.5319>
- Avants, B., Tustison, N. J., & Song, G. (2009). Advanced normalization tools: V1.0. *The Insight Journal*, *2*(365), 1–35. <https://doi.org/10.54294/uvnhin>
- Bakker, R., Tiesinga, P., & Kötter, R. (2015). The scalable brain atlas: Instant web-based access to public brain atlases and related content. *Neuroinformatics*, *13*(3), 353–366. <https://doi.org/10.1007/s12021-014-9258-x>
- Brett, M., Markiewicz, C. J., Hanke, M., Côté, M.-A., Cipollini, B., McCarthy, P., Jarecka, D., Cheng, C. P., Halchenko, Y. O., Cottaar, M., Larson, E., Ghosh, S., Wassermann, D., Gerhard, S., Lee, G. R., Baratz, Z., Wang, H.-T., Kastman, E., Kaczmarzyk, J., ... Reddam, V. R. (2023). *nipy/nibabel: 5.1.0* (5.1.0). Zenodo. <https://doi.org/10.5281/zenodo.7795644>
- Choi, H., Kim, Y. K., Yoon, E. J., Lee, J.-Y., Lee, D. S., & Alzheimer's Disease Neuroimaging Initiative. (2020). Cognitive signature of brain FDG PET based on deep learning: Domain transfer from Alzheimer's disease to Parkinson's disease. *European Journal of Nuclear Medicine and Molecular Imaging*, *47*(2), 403–412. <https://doi.org/10.1007/s00259-019-04538-7>
- Ding, Y., Sohn, J. H., Kawczynski, M. G., Trivedi, H., Harnish, R., Jenkins, N. W., Lituiev, D., Copeland, T. P., Aboian, M. S., Mari Aparici, C., Behr, S. C., Flavell, R. R., Huang, S.-Y., Zalocusky, K. A., Nardo, L., Seo, Y., Hawkins, R. A., Hernandez Pampaloni, M., Hadley, D., & Franc, B. L. (2019). A deep learning model to predict a diagnosis of Alzheimer disease by using F-FDG PET of the brain. *Radiology*, *290*(2), 456–464. <https://doi.org/10.1148/radiol.2018180958>
- Dyrba, M., Hanzig, M., Altenstein, S., Bader, S., Ballarini, T., Brosseron, F., Buerger, K., Cantré, D., Dechent, P., Dobisch, L., Düzel, E., Ewers, M., Fliessbach, K., Glanz, W., Haynes, J.-D., Heneka, M. T., Janowitz, D., Keles, D. B., Kilimann, I., ... Teipel, S. J. (2021). Improving 3D convolutional neural network comprehensibility via interactive visualization of relevance maps: Evaluation in Alzheimer's disease. *Alzheimer's Research & Therapy*, *13*(1), 191. <https://doi.org/10.1186/s13195-021-00924-2>
- Erickson, K. I., Donofry, S. D., Sewell, K. R., Brown, B. M., & Stillman, C. M. (2022). Cognitive aging and the promise of physical activity. *Annual Review of Clinical Psychology*, *18*, 417–442. <https://doi.org/10.1146/annurev-clinpsy-072720-014213>
- Hake, A., Trzepacz, P. T., Wang, S., Yu, P., Case, M., Hochstetler, H., Witte, M. M., Degenhardt, E. K., Dean, R. A., & Alzheimer's Disease Neuroimaging Initiative. (2015). Flortbetapir positron emission tomography and cerebrospinal fluid biomarkers. *Alzheimer's & Dementia*, *11*(8), 986–993. <https://doi.org/10.1016/j.jalz.2015.03.002>
- Hampel, H., Au, R., Mattke, S., van der Flier, W. M., Aisen, P., Apostolova, L., Chen, C., Cho, M., De Santi, S., Gao, P., Iwata, A., Kurzman, R., Saykin, A. J., Teipel, S., Vellas, B., Vergallo, A., Wang, H., & Cummings, J. (2022). Designing the next-generation clinical care pathway for Alzheimer's disease. *Nature Aging*, *2*(8), 692–703. <https://doi.org/10.1038/s43587-022-00269-x>
- Hampel, H., Cummings, J., Blennow, K., Gao, P., Jack, C. R. Jr., & Vergallo, A. (2021). Developing the ATX(N) classification for use across the Alzheimer disease continuum. *Nature Reviews. Neurology*, *17*(9), 580–589. <https://doi.org/10.1038/s41582-021-00520-w>
- Hampel, H., Hardy, J., Blennow, K., Chen, C., Perry, G., Kim, S. H., Villemagne, V. L., Aisen, P., Vendruscolo, M., Iwatsubo, T., Masters, C. L., Cho, M., Lannfelt, L., Cummings, J. L., & Vergallo, A. (2021). The amyloid- β pathway in Alzheimer's disease. *Molecular Psychiatry*, *26*(10), 5481–5503. <https://doi.org/10.1038/s41380-021-01249-0>
- He, K., Zhang, X., Ren, S., & Sun, J. (2016). *Deep residual learning for image recognition*. Proceedings of the IEEE conference on computer vision and pattern recognition (pp. 770–778).
- Heeman, F., Hendriks, J., Alves, I. L., Ossenkuppele, R., Tolboom, N., van Berckel, B. N. M., Lammertsma, A. A., Yaqub, M., & on behalf of the AMYPAD Consortium. (2020). [11C] PIB amyloid quantification: Effect of reference region selection. *EJNMMI Research*, *10*(1), 123. <https://doi.org/10.1186/s13550-020-00714-1>
- Insel, P. S., Mormino, E. C., Aisen, P. S., Thompson, W. K., & Donohue, M. C. (2020). Neuroanatomical spread of amyloid β and tau in Alzheimer's disease: Implications for primary prevention. *Brain Communications*, *2*(1), fcaa007. <https://doi.org/10.1093/braincomms/fcaa007>
- Jack, C. R. Jr., Albert, M. S., Knopman, D. S., McKhann, G. M., Sperling, R. A., Carrillo, M. C., Thies, B., & Phelps, C. H. (2011). Introduction to the recommendations from the National Institute on Aging-Alzheimer's Association workgroups on diagnostic guidelines for Alzheimer's disease. *Alzheimer's & Dementia: the Journal of the Alzheimer's Association*, *7*(3), 257–262. <https://doi.org/10.1016/j.jalz.2011.03.004>
- Jack, C. R. Jr., Bennett, D. A., Blennow, K., Carrillo, M. C., Dunn, B., Haeblerlein, S. B., Holtzman, D. M., Jagust, W., Jessen, F., Karlawish, J., Liu, E., Molinuevo, J. L., Montine, T., Phelps, C., Rankin, K. P., Rowe, C. C., Scheltens, P., Siemers, E., Snyder, H. M., ... Silverberg, N. (2018). NIA-AA research framework: Toward a biological definition of Alzheimer's disease. *Alzheimer's & Dementia: the Journal of the Alzheimer's Association*, *14*(4), 535–562. <https://doi.org/10.1016/j.jalz.2018.02.018>
- Jack, C. R., Knopman, D. S., Jagust, W. J., Shaw, L. M., Aisen, P. S., Weiner, M. W., Petersen, R. C., & Trojanowski, J. Q. (2010). Hypothetical model of dynamic biomarkers of the Alzheimer's pathological cascade. *The Lancet Neurology*, *9*(1), 119–128. [https://doi.org/10.1016/S1474-4422\(09\)70299-6](https://doi.org/10.1016/S1474-4422(09)70299-6)
- Jack, C. R. Jr., Wiste, H. J., Lesnick, T. G., Weigand, S. D., Knopman, D. S., Vemuri, P., Pankratz, V. S., Senjem, M. L., Gunter, J. L., Mielke, M. M., Lowe, V. J., Boeve, B. F., & Petersen, R. C. (2013). Brain β -amyloid load approaches a plateau. *Neurology*, *80*(10), 890–896. <https://doi.org/10.1212/WNL.0b013e3182840bbe>
- Jo, T., Nho, K., Risacher, S. L., Saykin, A. J., & Alzheimer's Disease Neuroimaging Initiative. (2020). Deep learning detection of informative features in tau PET for Alzheimer's disease classification.

- BMC Bioinformatics*, 21(Suppl 21), 496. <https://doi.org/10.1186/s12859-020-03848-0>
- Jo, T., Nho, K., & Saykin, A. J. (2019). Deep learning in Alzheimer's disease: Diagnostic classification and prognostic prediction using neuroimaging data. *Frontiers in Aging Neuroscience*, 11, 220. <https://doi.org/10.3389/fnagi.2019.00220>
- Johnson, K. A., Minoshima, S., Bohnen, N. I., Donohoe, K. J., Foster, N. L., Herscovitch, P., Karlawish, J. H., Rowe, C. C., Carrillo, M. C., Hartley, D. M., Hedrick, S., Pappas, V., Thies, W. H., & Alzheimer's Association, Society of Nuclear Medicine and Molecular Imaging, & Amyloid Imaging Taskforce. (2013). Appropriate use criteria for amyloid PET: A report of the amyloid imaging task force, the Society of Nuclear Medicine and Molecular Imaging, and the Alzheimer's Association. *Alzheimer's & Dementia: the Journal of the Alzheimer's Association*, 9(1), E1–E16.
- Kerbler, G. M., Fripp, J., Rowe, C. C., Villemagne, V. L., Salvado, O., Rose, S., Coulson, E. J., & Alzheimer's Disease Neuroimaging Initiative. (2015). Basal forebrain atrophy correlates with amyloid β burden in Alzheimer's disease. *NeuroImage. Clinical*, 7, 105–113. <https://doi.org/10.1016/j.nicl.2014.11.015>
- Kim, J.-Y., Suh, H. Y., Ryoo, H. G., Oh, D., Choi, H., Paeng, J. C., Cheon, G. J., Kang, K. W., Lee, D. S., & Alzheimer's Disease Neuroimaging Initiative. (2019). Amyloid PET quantification via end-to-end training of a deep learning. *Nuclear Medicine and Molecular Imaging*, 53(5), 340–348. <https://doi.org/10.1007/s13139-019-00610-0>
- Kinahan, P. E., & Fletcher, J. W. (2010). Positron emission tomography-computed tomography standardized uptake values in clinical practice and assessing response to therapy. *Seminars in Ultrasound, CT, and MR*, 31(6), 496–505. <https://doi.org/10.1053/j.sult.2010.10.001>
- Kingma, D. P., & Ba, J. (2014). Adam: A method for stochastic optimization. *arXiv Preprint. arXiv:1412.6980*
- Klunk, W. E., Engler, H., Nordberg, A., Wang, Y., Blomqvist, G., Holt, D. P., Bergström, M., Savitcheva, I., Huang, G.-F., Estrada, S., Ausén, B., Debnath, M. L., Barletta, J., Price, J. C., Sandell, J., Lopresti, B. J., Wall, A., Koivisto, P., Antoni, G., ... Långström, B. (2004). Imaging brain amyloid in Alzheimer's disease with Pittsburgh compound-B. *Annals of Neurology*, 55(3), 306–319. <https://doi.org/10.1002/ana.20009>
- Klunk, W. E., Koeppe, R. A., Price, J. C., Benzinger, T. L., Devous, M. D. Sr., Jagust, W. J., Johnson, K. A., Mathis, C. A., Minhas, D., Pontecorvo, M. J., Rowe, C. C., Skovronsky, D. M., & Mintun, M. A. (2015). The Centiloid project: Standardizing quantitative amyloid plaque estimation by PET. *Alzheimer's & Dementia: the Journal of the Alzheimer's Association*, 11(1), 1–15. <https://doi.org/10.1016/j.jalz.2014.07.003>
- Knopman, D. S., Parisi, J. E., Salviati, A., Floriach-Robert, M., Boeve, B. F., Ivnik, R. J., Smith, G. E., Dickson, D. W., Johnson, K. A., Petersen, L. E., McDonald, W. C., Braak, H., & Petersen, R. C. (2003). Neuropathology of cognitively normal elderly. *Journal of Neuropathology & Experimental Neurology*, 62(11), 1087–1095. <https://doi.org/10.1093/jnen/62.11.1087>
- Landau, S. M., Fero, A., Baker, S. L., Koeppe, R., Mintun, M., Chen, K., Reiman, E. M., & Jagust, W. J. (2015). Measurement of longitudinal β -amyloid change with 18F-florbetapir PET and standardized uptake value ratios. *Journal of Nuclear Medicine: Official Publication, Society of Nuclear Medicine*, 56(4), 567–574. <https://doi.org/10.2967/jnumed.114.148981>
- Lin, E., Lin, C.-H., & Lane, H.-Y. (2021). Deep learning with neuroimaging and genomics in Alzheimer's disease. *International Journal of Molecular Sciences*, 22(15), 7911. <https://doi.org/10.3390/ijms22157911>
- Matsubara, K., Ibaraki, M., Shimada, H., Ikoma, Y., Suhara, T., Kinoshita, T., & Ito, H. (2016). Impact of spillover from white matter by partial volume effect on quantification of amyloid deposition with [11C] PiB PET. *NeuroImage*, 143, 316–324. <https://doi.org/10.1016/j.neuroimage.2016.09.028>
- Mattsson, N., Palmqvist, S., Stomrud, E., Vogel, J., & Hansson, O. (2019). Staging β -amyloid pathology with amyloid positron emission tomography. *JAMA Neurology*, 76(11), 1319–1329. <https://doi.org/10.1001/jamaneurol.2019.2214>
- McKhann, G., Drachman, D., Folstein, M., Katzman, R., Price, D., & Stadlan, E. M. (1984). Clinical diagnosis of Alzheimer's disease: Report of the NINCDS-ADRDA work group under the auspices of Department of Health and Human Services Task Force on Alzheimer's Disease. *Neurology*, 34(7), 939–944. <https://doi.org/10.1212/WNL.34.7.939>
- Nelson, P. T., Head, E., Schmitt, F. A., Davis, P. R., Neltner, J. H., Jicha, G. A., Abner, E. L., Smith, C. D., Van Eldik, L. J., Kryscio, R. J., & Scheff, S. W. (2011). Alzheimer's disease is not “brain aging”: Neuropathological, genetic, and epidemiological human studies. *Acta Neuropathologica*, 121(5), 571–587. <https://doi.org/10.1007/s00401-011-0826-y>
- Niemantsverdriet, E., Ottoy, J., Somers, C., De Roeck, E., Struyfs, H., Soetewey, F., Verhaeghe, J., Van den Bossche, T., Van Mossevelde, S., Goeman, J., De Deyn, P. P., Mariën, P., Versijpt, J., Sleegers, K., Van Broeckhoven, C., Wyffels, L., Albert, A., Ceysens, S., Stroobants, S., ... Engelborghs, S. (2017). The cerebrospinal fluid A β 1-42/A β 1-40 ratio improves concordance with amyloid-PET for diagnosing Alzheimer's disease in a clinical setting. *Journal of Alzheimer's Disease: JAD*, 60(2), 561–576. <https://doi.org/10.3233/JAD-170327>
- Palmqvist, S., Zetterberg, H., Mattsson, N., Johansson, P., Alzheimer's Disease Neuroimaging Initiative, Minthon, L., Blennow, K., Olsson, M., Hansson, O., & Swedish BioFINDER Study Group. (2015). Detailed comparison of amyloid PET and CSF biomarkers for identifying early Alzheimer disease. *Neurology*, 85(14), 1240–1249. <https://doi.org/10.1212/WNL.0000000000001991>
- Pawlowski, N., Ktena, S. I., Lee, M. C., Kainz, B., Rueckert, D., Glocker, B., & Rajchl, M. (2017). Dltk: State of the art reference implementations for deep learning on medical images. *arXiv Preprint. arXiv:1711.06853*
- Petersen, R. C., Aisen, P. S., Beckett, L. A., Donohue, M. C., Gamst, A. C., Harvey, D. J., Jack, C. R. Jr., Jagust, W. J., Shaw, L. M., Toga, A. W., Trojanowski, J. Q., & Weiner, M. W. (2010). Alzheimer's Disease Neuroimaging Initiative (ADNI): Clinical characterization. *Neurology*, 74(3), 201–209. <https://doi.org/10.1212/WNL.0b013e3181cb3e25>
- Reith, F., Koran, M. E., Davidzon, G., Zaharchuk, G., & Alzheimer's Disease Neuroimaging Initiative. (2020). Application of deep learning to predict standardized uptake value ratio and amyloid status on F-Florbetapir PET using ADNI data. *AJNR. American Journal of Neuroradiology*, 41(6), 980–986. <https://doi.org/10.3174/ajnr.A6573>

- Reith, F. H., Mormino, E. C., & Zaharchuk, G. (2021). Predicting future amyloid biomarkers in dementia patients with machine learning to improve clinical trial patient selection. *Alzheimer's & Dementia: the Journal of the Alzheimer's Association*, 7(1), e12212. <https://doi.org/10.1002/trc2.12212>
- Richards, D., & Sabbagh, M. N. (2014). Flortetaben for PET imaging of beta-amyloid plaques in the brain. *Neurology and Therapy*, 3(2), 79–88. <https://doi.org/10.1007/s40120-014-0022-9>
- Rieke, J., Eitel, F., Weygandt, M., Haynes, J. D., & Ritter, K. (2018). Visualizing convolutional networks for MRI-based diagnosis of Alzheimer's disease. In *Understanding and interpreting machine learning in medical image computing applications: First international workshops, MLCN 2018, DLF 2018, and iMIC 2018, held in conjunction with MICCAI 2018, Granada, Spain, September 16–20, 2018, proceedings 1* (pp. 24–31). Springer International Publishing.
- Shah, J., Gao, F., Li, B., Ghisays, V., Luo, J., Chen, Y., Lee, W., Zhou, Y., Benzinger, T. L. S., Reiman, E. M., Chen, K., Su, Y., & Wu, T. (2022). Deep residual inception encoder-decoder network for amyloid PET harmonization. *Alzheimer's & Dementia: the Journal of the Alzheimer's Association*, 18(12), 2448–2457. <https://doi.org/10.1002/alz.12564>
- Shaw, L. M., & Trojanowski, J. Q. (2017). *Biomarker Core report: Year1 ADNI3, Roche Elecsys immunoassay analyses of ADNI1/GO/2 CSF samples*. Alzheimer's Association. <https://www.alz.org/media/documents/ww-adni-may-2017-biomarker-core-shaw.pdf>
- Shaw, L. M., Vanderstichele, H., Knapik-Czajka, M., Clark, C. M., Aisen, P. S., Petersen, R. C., Blennow, K., Soares, H., Simon, A., Lewczuk, P., Dean, R., Siemers, E., Potter, W., Lee, V. M.-Y., Trojanowski, J. Q., & Alzheimer's Disease Neuroimaging Initiative. (2009). Cerebrospinal fluid biomarker signature in Alzheimer's disease neuroimaging initiative subjects. *Annals of Neurology*, 65(4), 403–413. <https://doi.org/10.1002/ana.21610>
- Soret, M., Bacharach, S. L., & Buvat, I. (2007). Partial-volume effect in PET tumor imaging. *Journal of Nuclear Medicine: Official Publication, Society of Nuclear Medicine*, 48(6), 932–945. <https://doi.org/10.2967/jnumed.106.035774>
- Spallazzi, M., Barocco, F., Michelini, G., Immovilli, P., Taga, A., Morelli, N., Ruffini, L., & Caffarra, P. (2019). CSF biomarkers and amyloid PET: Concordance and diagnostic accuracy in a MCI cohort. *Acta Neurologica Belgica*, 119(3), 445–452. <https://doi.org/10.1007/s13760-019-01112-8>
- Sperling, R. A., Karlawish, J., & Johnson, K. A. (2013). Preclinical Alzheimer disease—The challenges ahead. *Nature Reviews. Neurology*, 9(1), 54–58. <https://doi.org/10.1038/nrneurol.2012.241>
- Springenberg, J. T., Dosovitskiy, A., Brox, T., & Riedmiller, M. (2014). Striving for simplicity: The All Convolutional Net. <https://doi.org/10.48550/arXiv.1412.6806>
- Teipel, S. J., Cavado, E., Hampel, H., Grothe, M. J., & Alzheimer's Disease Neuroimaging Initiative, & Alzheimer Precision Medicine Initiative (APMI). (2018). Basal forebrain volume, but not hippocampal volume, is a predictor of global cognitive decline in patients with Alzheimer's disease treated with cholinesterase inhibitors. *Frontiers in Neurology*, 9, 642. <https://doi.org/10.3389/fneur.2018.00642>
- Thal, D. R., Rüb, U., Orantes, M., & Braak, H. (2002). Phases of A β deposition in the human brain and its relevance for the development of AD. *Neurology*, 58(12), 1791–1800. <https://doi.org/10.1212/WNL.58.12.1791>
- Weber, C. J., Carrillo, M. C., Jagust, W., Jack, C. R. Jr., Shaw, L. M., Trojanowski, J. Q., Saykin, A. J., Beckett, L. A., Sur, C., Rao, N. P., Mendez, P. C., Black, S. E., Li, K., Iwatsubo, T., Chang, C.-C., Sosa, A. L., Rowe, C. C., Perrin, R. J., Morris, J. C., ... Weiner, M. W. (2021). The worldwide Alzheimer's Disease Neuroimaging Initiative: ADNI-3 updates and global perspectives. *Alzheimer's & Dementia: the Journal of the Alzheimer's Association*, 7(1), e12226. <https://doi.org/10.1002/trc2.12226>
- Wolk, D. A., Zhang, Z., Boudhar, S., Clark, C. M., Pontecorvo, M. J., & Arnold, S. E. (2012). Amyloid imaging in Alzheimer's disease: Comparison of flortetapir and Pittsburgh compound-B positron emission tomography. *Journal of Neurology, Neurosurgery, and Psychiatry*, 83(9), 923–926. <https://doi.org/10.1136/jnnp-2012-302548>

SUPPORTING INFORMATION

Additional supporting information can be found online in the Supporting Information section at the end of this article.

How to cite this article: Tagmazian, A. A., Schwarz, C., Lange, C., Pitkänen, E., Vuoksimaa, E., & for the Alzheimer's Disease Neuroimaging Initiative (2024). ArcheD, a residual neural network for prediction of cerebrospinal fluid amyloid-beta from amyloid PET images. *European Journal of Neuroscience*, 1–15. <https://doi.org/10.1111/ejn.16332>